

Hysteresis modeling of timber-based structural systems using a combined data and model-driven approach

Original

Hysteresis modeling of timber-based structural systems using a combined data and model-driven approach / Aloisio, A.; Rosso, M. M.; Iqbal, A.; Fragiacomò, M.. - In: COMPUTERS & STRUCTURES. - ISSN 0045-7949. - 269:(2022), p. 106830. [10.1016/j.compstruc.2022.106830]

Availability:

This version is available at: 11583/2972670 since: 2022-10-28T10:28:02Z

Publisher:

Elsevier

Published

DOI:10.1016/j.compstruc.2022.106830

Terms of use:

This article is made available under terms and conditions as specified in the corresponding bibliographic description in the repository

Publisher copyright

Elsevier postprint/Author's Accepted Manuscript

© 2022. This manuscript version is made available under the CC-BY-NC-ND 4.0 license
<http://creativecommons.org/licenses/by-nc-nd/4.0/>. The final authenticated version is available online at:
<http://dx.doi.org/10.1016/j.compstruc.2022.106830>

(Article begins on next page)

Hysteresis modeling of timber-based structural systems using a combined data and model-driven approach

Angelo Aloisio^{a,*}, Marco Martino Rosso^b, Asif Iqbal^c, Massimo Fragiaco^a

^a*Civil and Environmental Engineering Department, Università degli Studi dell'Aquila, L'Aquila, 67100, Italy*

^b*Politecnico di Torino, DISEG, Dipartimento di Ingegneria Strutturale, Edile e Geotecnica, Corso Duca Degli Abruzzi, 24, Turin, 10128, Italy*

^c*Department of Civil Engineering, University of Northern British Columbia, Prince George, Canada*

^d*Department of Civil, Construction-Architectural and Environmental Engineering, Università degli Studi dell'Aquila, Via G. Gronchi, 18, L'Aquila, 67100, Abruzzo, Italy*

Abstract

This paper presents a novel computational approach to empirical hysteresis modelling applied to timber-based structures based on a combined data model-driven strategy. While the backbone curve is simulated using the experimental cyclic response based on a step-by-step optimization problem (data-driven approach), analytical functions describe the re-loading curves (model-driven approach). Empirical hysteresis models developed so far for timber structures are model-driven. However, the backbone curves can exhibit a highly irregular non-smooth trend, difficult to mirror using analytical formulations. The challenge in mirroring the experimental backbone using closed-form formulations has led to an extended set of parameters to be calibrated in existing literature models. This paper presents a novel approach to the empirical hysteresis model, where the experimental data are directly involved, as a whole, in the model formulation. This model aims to be a possible trade-off between model complexity and accuracy. A reduced number of parameters needed to describe the re-loading paths is counterbalanced using an entire subset of the experimental data. The paper delivers the developed Matlab and Python codes for further implementation as a user-defined element within a Finite Element software.

Keywords: Hysteresis models; timber engineering; shear walls; pinching; Cross-Lam timber; light-frame timber.

31 **1. Introduction**

32 Empirical hysteresis modelling is a branch of structural engineering devoted to
33 simulating structural systems' experimental cyclic response. Empirical hysteresis
34 models lack mechanical interpretation, blindly matching the experimental data [1].
35 There are differential and non-differential approaches to empirical hysteresis mod-
36 els. The most used differential models belong to the so-called Bouc-Wen class [1–5].
37 They are based on a first-order differential equation, representing the evolution of the
38 inelastic displacement response. After the first paper by Bouc [6], other researchers
39 presented modifications and extensions of the Bouc-Wen model to simulate asym-
40 metric hysteresis, degradation phenomena and pinching [7–11].
41 Non-differential models originate from a piece-wise definition of the hysteresis loop
42 [12–16]. The main differences between non-differential models stand in adopting
43 diverse analytical functions for each section of the loop and proper continuity condi-
44 tions. Most of the research in structural engineering, chiefly directed on applications,
45 does not deal with differential hysteresis models more evolved than the Bouc-Wen
46 class ones and focalizes on non-differential formulations due to flaws and challenges
47 in using these models [7, 17–19].
48 In the last two decades, timber engineering experienced significant advancement in
49 the development of non-differential models, featured by some stability advantages
50 to the differential ones: they are generally faster and less computationally demand-
51 ing. The primary objective in using empirical hysteresis modelling rather than finite
52 elements is to simulate extended structural arrangements with multiple connections
53 [3, 19–23]. The finite element modelling of each connection, where most dissipation
54 is confined, may lead to a high computational cost [24–29]. Therefore, the mod-
55 elling of a real-case structural arrangement with multiple dissipation sources entails

*Corresponding author.

Email address: `angelo.aloisio1@univaq.it` (Angelo Aloisio)

56 impractical finite element simulations due to the time length of the analysis. The
57 development of reliable hysteresis models represents a crucial issue to reduce the du-
58 ration of simulations [30–33]. The main differences between non-differential models
59 stand in the definition of the piece-wise functions. There is the model by Polensek
60 and Laursen [34] based on linear functions, the trilinear model by Rinaldin et al.
61 [35] and the SAWS Material Model (OpenSees) [36]. Conversely, the CUREE model
62 [37], the evolutionary parameter hysteretic model (EPHM) [38] and others [39, 40]
63 present nonlinear branches. Dolan [41, 42] developed a transcendental hysteresis
64 model based on four exponential functions that define the hysteretic curves. For a
65 concise literature review of empirical hysteresis models for timber-based structural
66 systems, the reader can refer to [43].

67 So far, no scholar proposed a hybrid approach to hysteresis, where the exper-
68 imental data, not just their optimum fitting, participate in the model definition.
69 Interestingly, while the backbone curves of timber-based assemblies exhibit a non-
70 regular progression, the re-loading and un-loading curves present a more smooth
71 trend, see in Fig.1 the cyclic response of a Cross-Laminated Timber shear wall. The
72 main challenge in hysteresis modelling is the calibration of the degradation param-
73 eters for an optimum fitting of the backbone curve. The number of parameters
74 boosts if the backbone curve is so irregular that the scholar must use a piece-wise
75 definition of each loading path. Therefore, the model may grow in complexity due
76 to the difficulties in mirroring the irregular backbone (abrupt strength decay, wavy
77 trend, e.g.). Several models achieve a good fitting of the maximum force, neglecting
78 the matching between simulated and real force values at lower displacement [43].
79 The empirical hysteresis model’s goal is to achieve an almost exact correspondence
80 between experimental and numerical data. Still, the erratic nature of the backbone
81 curve requires specific analytical functions depending on the particular system un-
82 der investigation. Accordingly, in this paper, the authors propose a hybrid approach
83 to hysteresis. The first-loading curves (backbone) do not descend from analytical

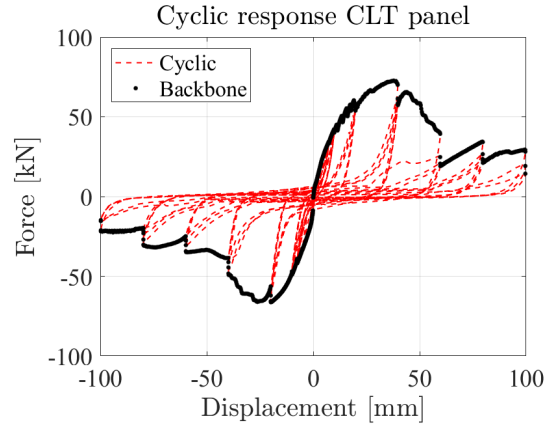


Figure 1: Experimental cyclic response of a Cross-Laminated Timber shear wall. The experimental tests are detailed in [44, 45].

84 functions but directly arise from a step-by-step optimization of the experimental
 85 backbone. Conversely, the re-loading and un-loading paths, exhibiting a smoother
 86 trend, have a straightforward definition based on power functions. The resulting hys-
 87 teresis model could be advantageous to the reduced number of unknown parameters:
 88 the residual force at zero displacements and the exponents of the power functions.
 89 The authors observed that this model satisfactorily reproduces a set of experimental
 90 data expressing the variability of hysteresis on timber engineering. The calibration
 91 of the parameters is straightforward and does not require dedicated optimization. It
 92 can also originate from hand-tuning in practice-oriented circumstances due to their
 93 reduced variability and mutual correlation. The chief task in empirical hysteresis
 94 modelling can be to simulate the backbone curve: this issue is solved by directly
 95 adopting the experimental force values. The experimental data are always required
 96 for proper model calibration and are frequently available to the scholar who carries
 97 out structural analyses.

98 Therefore, the proposed formulation has two pieces of novelties compared to existing
 99 ones. (i) The inclusion of the experimental backbone, leading to a hybrid, analytical-
 100 numerical hysteresis model. (ii) Adopting the sole maximum displacement as an
 101 evolutionary parameter, ignoring the dependence on dissipated hysteretic energy.

102 The paper discusses the feasibility of a hybrid approach to empirical hysteresis

103 modelling based on a data/model-driven strategy. The second section presents the
 104 mathematical formulation of the hysteresis model, while the third section addresses
 105 the fitting capacity of the model on a chosen dataset. The fourth section deals with
 106 the model validation using the experimental cyclic response of a given structure
 107 under different loading protocols. The last section gives concluding remarks about
 108 the current model development. The Appendix reports the complete MATLAB and
 109 Python codes developed by the authors for possible use by other researchers.

110 2. Hysteresis model formulation

111 The current hysteresis model originates from a heterogeneous formulation. The
 112 backbone curve, which delimits the upper and lower bounds of hysteresis, derives
 113 from an optimization problem based on the experimental cyclic response of the
 114 structural system. The re-loading and unloading curves are power functions whose
 115 coefficients derive from the fulfillment of the continuity conditions, while the ex-
 116 ponent depending on the curvature of the experimental curves. Eq.(1) collects the
 117 experimental backbone:

$$\begin{aligned}
 \mathbf{d}^+ &= \{d_1^+, \dots, d_i^+, \dots, d_n^+\} \\
 \mathbf{f}^+ &= \{f_1^+, \dots, f_i^+, \dots, f_n^+\} \\
 \mathbf{d}^- &= \{d_1^-, \dots, d_i^-, \dots, d_m^-\} \\
 \mathbf{f}^- &= \{f_1^-, \dots, f_i^-, \dots, f_m^-\}
 \end{aligned} \tag{1}$$

118 where d^+ and d^- are the positive and negative displacements associated to the
 119 positive \mathbf{f}^+ and negative \mathbf{f}^- force values. Fig.2 illustrates the main idea behind the
 120 proposed formulation. The hysteresis loop consists of six different phases, identified
 121 by the sign of velocity, displacement, and the past displacement history. The authors
 122 did not include the force value in the definition of hysteresis to achieve a more
 123 stable transition between phases. The force value is unknown in displacement-driven
 124 simulations and cannot be swiftly included in the conditional statements defining
 125 the transition phases.

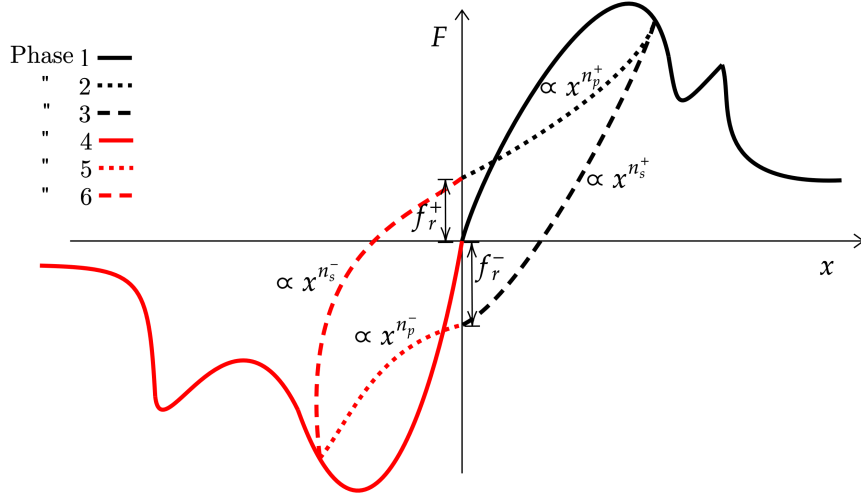


Figure 2: Definition of the hysteresis cycle based on the definition of six phases, identified by the sign of the displacement and velocity, and the occurring of pinching.

- 126 1. The first phase corresponds to the positive backbone, characterized by positive
127 displacements, positive velocity and displacement higher than the maximum
128 attained in the past history. The k th force value originates from the mini-
129 mization of the squared difference between the k th simulated displacement x_k
130 and the experimental displacement vector \mathbf{d}^+ . The minimum argument of the
131 resulting vector corresponds to the index of the optimum experimental force
132 value, \mathbf{f}^+ .
- 133 2. The second phase corresponds to the re-loading curve, characterized by posi-
134 tive displacements, positive velocity and displacement lower than the maxi-
135 mum attained in the past history. A power function with n_p^+ exponent defines
136 the evolution of the resisting force. The coefficient is tuned to yield a force
137 value corresponding to the maximum displacement attained in the past his-
138 tory. Accordingly, the stiffness of the pinching path depends on the maximum
139 attained displacement. Therefore, the coefficient is variable and derives from
140 step-by-step optimization similar to the one described in phase 1.
- 141 3. The third phase corresponds to the un-loading curve, characterized by posi-
142 tive displacements and negative velocity. A power function with n_s^+ exponent

143 defines the evolution of the resisting force. The coefficient is tuned to yield
144 a force value corresponding to the maximum argument of the relative maxi-
145 mum displacement attained in the past history. Accordingly, the stiffness of
146 this path depends on the fulfilment of the continuity between loading and un-
147 loading, imposing the identity of the force value. Therefore, the coefficient is
148 variable and descends from step-by-step optimization based on the simulated
149 data up to the k th integration step.

150 4. The fourth phase corresponds to the negative backbone, characterized by neg-
151 ative displacements, positive velocity and displacement lower than the maxi-
152 mum attained in the past history. The k th force value originates from the min-
153 imization of the squared difference between the k th simulated displacement x_k
154 and the experimental displacement vector \mathbf{d}^- . The minimum argument of the
155 resulting vector corresponds to the index of the optimum experimental force
156 value, \mathbf{f}^- .

157 5. The fifth phase corresponds to the re-loading curve, characterized by negative
158 displacements, positive velocity and displacement higher than the maximum
159 attained in the past history. A power function with n_p^- exponent defines the
160 evolution of the resisting force. The coefficient is tuned to yield a force value
161 corresponding to the minimum displacement attained in the past history. Ac-
162 cordingly, the stiffness of the pinching path depends on the minimum attained
163 displacement. Therefore, the coefficient is variable and derives from step-by-
164 step optimization similar to the one described in phase 4.

165 6. The sixth phase corresponds to the un-loading curve, characterized by nega-
166 tive displacements and negative velocity. A power function with n_s^- exponent
167 defines the evolution of the resisting force. The coefficient is tuned to yield
168 a force value corresponding to the maximum argument of the relative mini-
169 mum displacement attained in the past history. Accordingly, the stiffness of
170 this path depends on the fulfilment of the continuity between loading and un-

171 loading, imposing the identity of the force value. Therefore, the coefficient is
 172 variable and descends from step-by-step optimization based on the simulated
 173 data up to the k th integration step.

174 The suggested hybrid formulation aims at reducing the number of unknown
 175 parameters by enhancing the model accuracy using the experimental cyclic response
 176 data. Eq.(2) collects into two vectors the input and output data. The input data
 177 are the positive and negative backbone values with additional six scalar parameters.
 178 The parameters can descend from a direct inspection of the experimental data or
 179 the solution of an optimization problem. Specifically, the n values identify the
 180 curvature of the power function, while f_r are the force values associated with zero
 181 displacements.

$$\begin{aligned} \text{Input} &= \{\mathbf{d}^+, \mathbf{d}^-, \mathbf{f}^+, \mathbf{f}^-, n_s^+, n_p^+, f_r^+, n_s^-, n_p^-, f_r^-\} \\ \text{Output} &= \{\mathbf{x}, \mathbf{f}\} \end{aligned} \quad (2)$$

182 The output data are the force and displacement vectors, \mathbf{f} and \mathbf{x} respectively. In
 183 displacement-driven simulations, the displacement is known and the outputs reduce
 184 to \mathbf{f} . Eq.(3) defines the displacement and force vectors up to the k th integration
 185 step, used in Eq.(4) for the formulation of the mathematical problem.

$$\begin{aligned} \mathbf{x}_k &= \{x_1, \dots, x_k\} \\ \mathbf{f}_k &= \{f_1, \dots, f_k\} \end{aligned} \quad (3)$$

186 Eq.(4), divided into six sections, represents the mathematical description of the

Phase 1

if $\{x_k - x_{k-1} \geq 0, x_k \geq 0, x_k \geq \max(\mathbf{x}_k)\}$

$$f_k = \mathbf{f}^+(\arg \min_i (x_k - \mathbf{d}^+)^2)$$

—

Phase 2

if $\{x_k - x_{k-1} \geq 0, x_k \geq 0, x_k < \max(\mathbf{x}_k)\}$

$$f_k = \frac{f_{\max} - f_r^+}{|\max(\mathbf{x}_k)|^{n_p^+}} |x_k|^{n_p^+} + f_r^+$$

$$f_{\max} = \mathbf{f}^+(\arg \min_i (\max(\mathbf{x}_k) - \mathbf{d}^+)^2)$$

—

Phase 3

if $\{x_k - x_{k-1} < 0, x_k \geq 0\}$

$$f_k = \frac{f_m - f_r^+}{|x_m|^{n_s^+}} |x_k|^{n_s^+} - f_r^+$$

$$f_m = f_{(\max(\arg \max_k (\Delta \mathbf{f}_k)))} | \Delta f_k = f_k - f_{k-1}$$

$$x_m = x_{(\max(\arg \max_k (\Delta \mathbf{x}_k)))} | \Delta x_k = x_k - x_{k-1}$$

—

(4)

Phase 4

if $\{x_k - x_{k-1} \geq 0, x_k < 0, x_k \leq \min(\mathbf{x}_k)\}$

$$f_k = \mathbf{f}^-(\arg \min_i (x_k - \mathbf{d}^-)^2)$$

—

Phase 5

if $\{x_k - x_{k-1} \geq 0, x_k < 0, x_k > \min(\mathbf{x}_k)\}$

$$f_k = \frac{f_{\max} - f_r^-}{|\max(\mathbf{x}_k)|^{n_p^-}} |x_k|^{n_p^-} - f_r^-$$

$$f_{\min} = \mathbf{f}^-(\arg \min_i (\min(\mathbf{x}_k) - \mathbf{d}^-)^2)$$

—

Phase 6

if $\{x_k - x_{k-1} < 0, x_k < 0\}$

$$f_k = \frac{f_l + f_r^-}{|x_l|^{n_s^-}} |x_k|^{n_s^-} + f_r^-$$

$$f_l = f_{(\max(\arg \min_k (\Delta \mathbf{f}_k)))} | \Delta f_k = f_k - f_{k-1}$$

$$x_l = x_{(\max(\arg \min_k (\Delta \mathbf{x}_k)))} | \Delta x_k = x_k - x_{k-1}$$

188 The authors implemented the model in Eq.(4) in Matlab. The associated code
189 is available to the scholar in the Appendix.

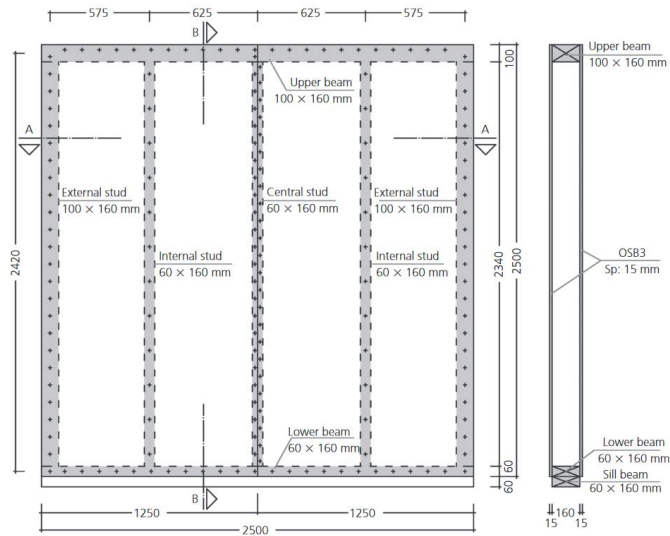
190 **3. Results: response under imposed displacement**

191 The authors estimated the fitting capacity of the proposed formulation with the
192 experimental cyclic response of three structural systems: a Light-Timber Framed
193 (LTF) and Cross-Laminated Timber (CLT) shear walls, and an angle bracket (AB).
194 The three structural responses exhibited diverse distinctiveness and were chosen to
195 estimate the performance of the proposed empirical hysteresis model. The dimen-
196 sion of the LTF shear wall is 2.5×2.5 m, see Fig.3(a). The test setup, shown in
197 Fig.3(b), followed the EN 594:2011 protocol. The experimental data refer to a spec-
198 imen with a vertical load equal to 20kN, two hold-downs, three angle brackets and
199 an OBS sheathing fastened by nails to the framed structure. The frame elements
200 are C24, with sections reported in Fig.3(a).

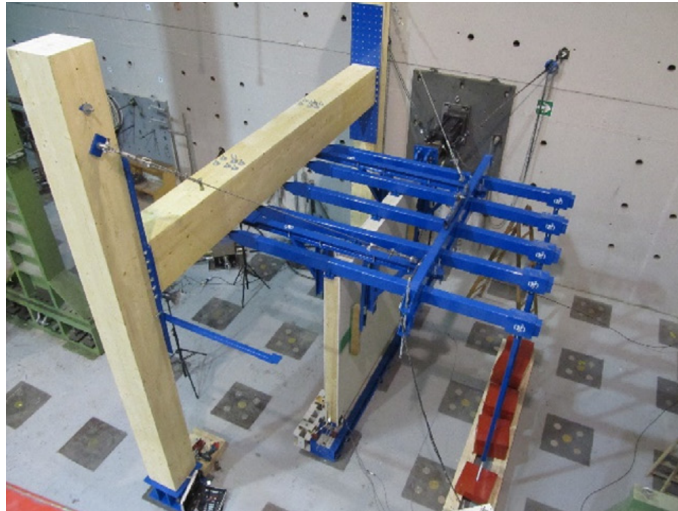
201 The CLT shear walls are 2.5×2.5 m, see Fig.4. They consist of three layers (thick-
202 ness 30-30-30 mm) of C24 boards. The experimental data refer to a specimen with
203 a vertical load equal to 20kN, two hold-downs and four angle brackets. The cyclic
204 test data of three CLT shear walls, labelled STDL0-L0, NA620-L20 and NAWH-L20
205 after [45], have been used. The reader can refer to [44, 45] for additional details
206 about the tested specimens and the experimental setup.

207 The Angle Bracket (AB) is a Reinforced Angle Bracket (105-R) - Simpson Strong-
208 Tie $105\text{mm} \times 105\text{mm} \times 90\text{mm}$. The experimental data refer to the shear response
209 of the AB.

210 Figs.6,7,8 depict the comparison between the experimental and simulated data
211 for the LTF, CLT and AB. The substantial symmetry of the experimental data
212 determined the reduction of the unknown parameters from six to three. They are the
213 residual force ($f_r = f_r^+ = f_r^-$) and the exponents of the power functions associated
214 with the re-loading ($n_p = n_p^+ = n_p^-$) and un-loading paths ($n_s = n_s^+ = n_s^-$). The



(a)



(b)

Figure 3: (a) Constructive details of the partially anchored LTF shear wall tested by [44, 45] and (b) a view of the experimental setup.

215 LTF manifests a progressive increment of the resisting force, the attainment of the
 216 maximum force close to 70kN and the force decaying at displacements higher than
 217 30mm. The re-loading and un-loading curves have quite regular evolution up to
 218 30mm, then the curve concavity changes in the last cycles. The n_p and n_s exponents
 219 are constant. Therefore, the least-square optimization of the unknown parameters
 220 led to a set of parameters closely following the experimental data up to 30mm. The
 221 pinching and un-loading paths of the last two cycles are associated with larger error
 222 due to n_p and n_s stationarity. Except for this inconsistency, the correspondence up

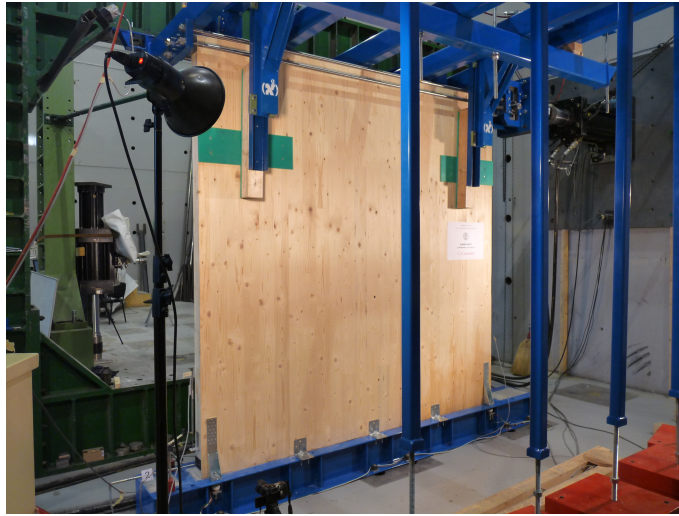


Figure 4: View of the CLT shear wall tested by [44, 45].



Figure 5: View of the angle bracket tested by the authors.

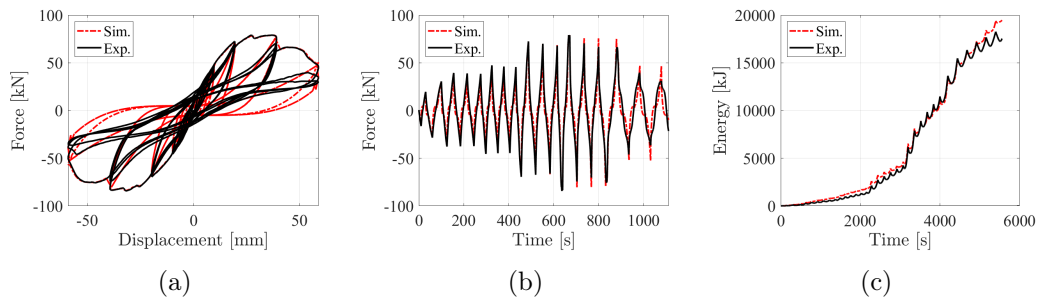


Figure 6: Comparison between the experimental cyclic response of a LTF shear wall and the proposed model in term of force-displacement (a), force-time (b) and energy-time (c) functions. Exp. stands for experimental data, while Sim. for simulated data.

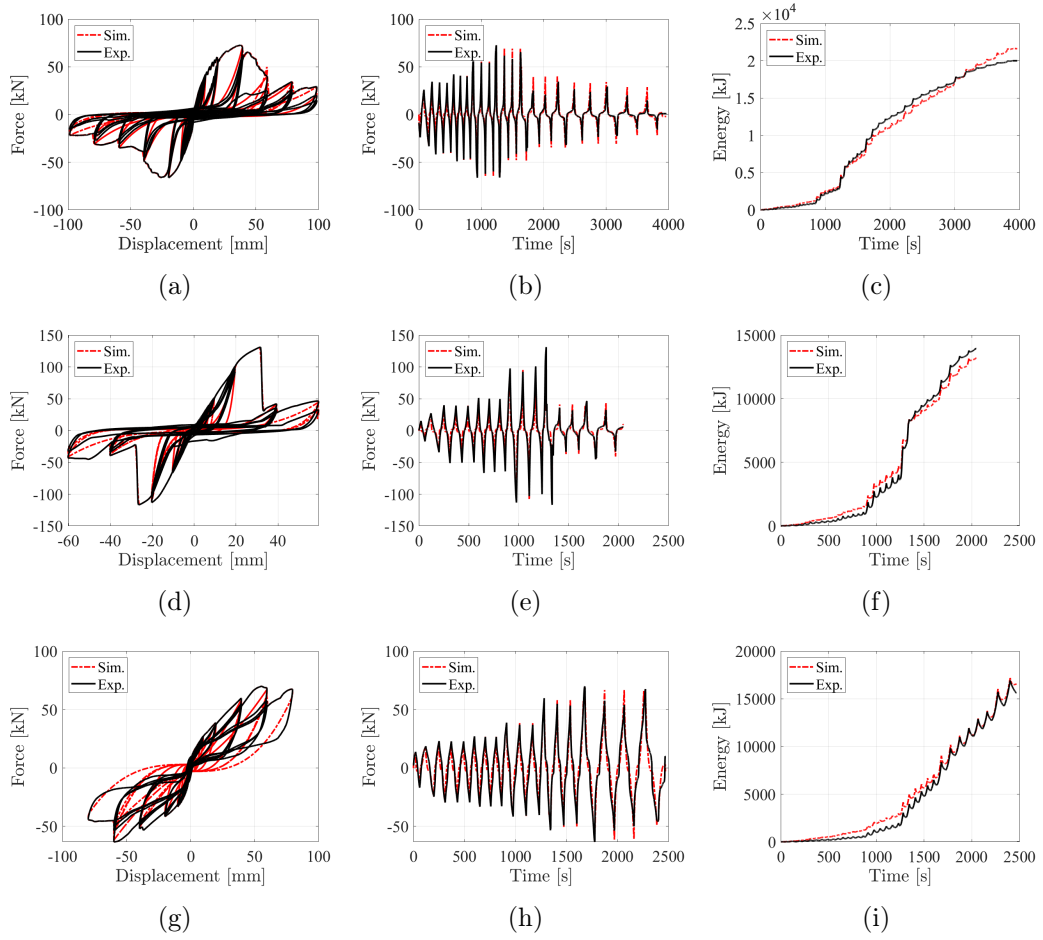


Figure 7: Comparison between the experimental cyclic response of three CLT shear walls (STDL0-L0 (a)-(c); NA620-L20 in (d)-(f); NAWH-L20 in (g)-(i), labelled after [45]) and the proposed model in term of force-displacement (a),(d), force-time (b),(e) and energy-time (c),(f) functions. Exp. stands for experimental data, while Sim. for simulated data.

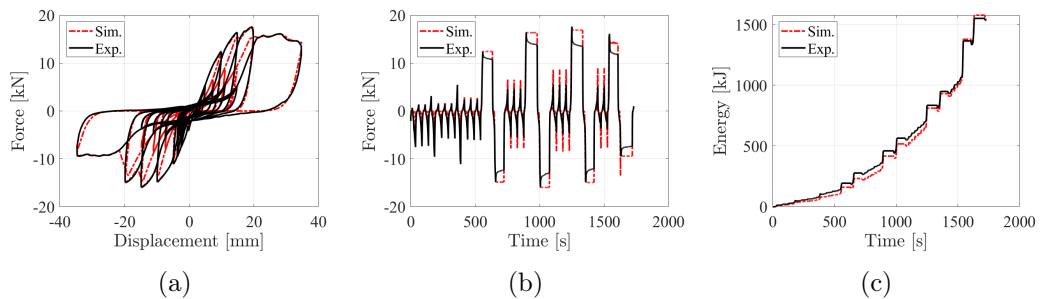


Figure 8: Comparison between the experimental cyclic response of an angle bracket and the proposed model, in term of force-displacement (a), force-time (b) and energy-time (c) functions. Exp. stands for experimental data, while Sim. for simulated data.

223 to 30mm is so accurate that it is difficult to distinguish the two superposed curves.
224 The backbone of CLT is more erratic, as evidenced from Fig.1. There is a steady
225 increment of the residual force, followed by an immediate decay due to the hold-
226 down failure. After the abrupt force decrement, the force upholds at a lower value.
227 In this circumstance, the re-loading and un-loading paths do not modify concavity,
228 and constant values of n_p and n_s yield a reliable matching.
229 The cyclic response of the angle bracket is also peculiar due to the notable difference
230 in the concavity of re-loading and un-loading. Still, this aspect is not an obstacle
231 for the presented formulation. A significant difference between the two n_p and n_s
232 exponents mirrors the gap in the concavity. Interestingly, stationary parameters,
233 like n_p and n_s , faithfully seize the variability of re-loading and unloading.

Table 1: Model parameters, Root Mean Square error (rmse) and maximum error corresponding to the models in Figs.6,7,8. The error is the difference between the experimental and simulated force vectors. The three values for the CLT panel refer to the three specimens STD-L0, NA620-L20 and NAWH-L20 labelled after [45].

Value	LTF	CLT	AB
$n_p^+ = n_p^-$	2.3	{3.5,3.1,1.5}	2.2
$n_s^+ = n_s^-$	4.2	{6.1,8.7,4.2}	13.9
$f_r^+ = f_r^-$ [kN]	5.11	{2.5,2.5,3.1}	2.1
Max error [kN]	37.34	{34.34, 45.47,43.21}	7.93
RMSE [kN]	9.7	{12.43, 20.12, 19.21}	1.37

234 Tab.1 shows the calibrated parameters of the three models, LTF CLT and AB,
235 obtained from a Least-Squares Optimization. The residual forces do not exhibit
236 substantial scatter and do not exceed the 10% of the maximum force. This aspect
237 is characteristic of timber-based structures and highlights the limited significance
238 of the residual force compared to other structural systems (rubber isolators, e.g.),
239 where the role of f_r is determinant being very close to the maximum force. The ex-
240 ponents express the concavity of re-loading and un-loading. The difference between
241 n_p and n_s leads to energy dissipation, corresponding to the area enclosed by the
242 two paths. In the three structural systems, the n_p exponent almost stands between
243 2 and 3. Conversely, the n_s exponent has a higher variability and represents a key
244 parameter affecting the differences in energy dissipation. It is approximately 4 in

245 LTF, 6 in CLT and boosts to 13.9 in AB.

246 Tab.1 also presents the Maximum Error (ME), which is the maximum difference
247 between the simulated and experimental force values, and the Root Mean Square
248 Error (RMSE). The RMS is always lower than the ME. It confirms that the model
249 is, on average, quite corresponding to the experimental data. Nevertheless, in a few
250 situations, the model strives to grasp the maximum force value due to nonstationary
251 pinching fractions. It may occur the ratio between the force in the backbone and
252 pinching path given a certain displacement is not constant. This occurrence can
253 lead to an error in the estimate of the peak force.

254

255 Fig.6,7,8 and Tab.1 proved that there is a good correspondence between the ex-
256 perimental and simulated data. Still, the main limitations stand in the stationarity
257 of the model parameters. Reasonably, the n exponents, the residual forces f_r and
258 the pinching fractions are not constant but dependent on the displacement history.
259 A higher matching can be achieved by selecting time-variant parameters. However,
260 the model represents a compromise between the adoption of limited parameters
261 and the model accuracy. The authors believe that despite the reduced number of
262 parameters, the model expresses a satisfactory level of accuracy for engineering
263 purposes.

264 Interestingly, the authors describe a degrading system with such limited parameters
265 by including the experimental backbone within the formulation. Many scholars pre-
266 sented hysteresis models with pinching and degradation with many parameters [3].
267 The parameters must express both the shape of hysteresis and the dependence on
268 the dissipated hysteretic energy. The dissipated hysteretic energy is the most used
269 parameter for the simulation of time-variant systems. The last section discusses the
270 role of dissipated energy in empirical hysteresis models.

271

272 The model displays a stable performance under non-stationary inputs (earth-

273 quake, e.g.) when the displacement vector is unknown and descends from the so-
 274 lution of a second-order nonlinear differential equation. The authors examine the
 275 model performance by modelling the structural response of the LTF archetype as
 276 Single-Degree-Of-Freedom (SDOF) systems. The following nonlinear ordinary dif-
 277 ferential equation describes the cyclic response of the LTF shear wall modelled as a
 278 SDOF system. The model has a lumped mass by the top, while the resisting force
 279 is the defined hysteresis model. The explicit fourth-order Runge–Kutta method is
 280 used for the temporal discretization of Eq's approximate solution (5).

$$m\ddot{x} + f_s = -m\ddot{x}_g \quad (5)$$

281 where m is the mass, x the displacement, \ddot{x} the double derivative of x with respect
 282 to time, f_s the resisting inelastic force, and \ddot{x}_g the ground acceleration. In the
 283 considered SDOF system, the mass $m = 1\text{ton}$.

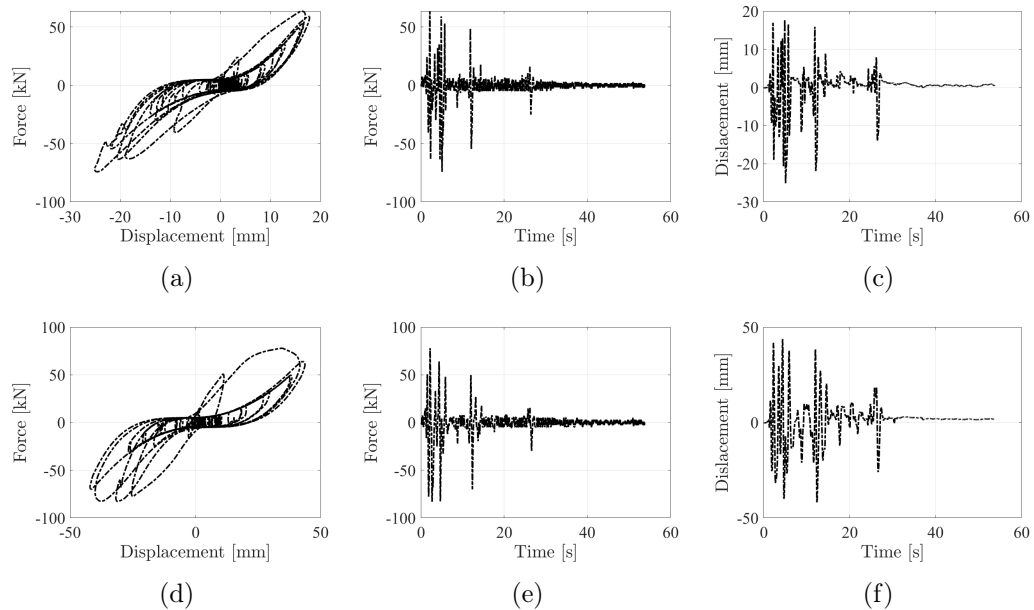


Figure 9: Integration of Eq.5 under El Centro earthquake with $m=10\text{ton}$, where the resisting force is the LTF model depicted in Fig.6. Plot of the force-displacement (a)-(d), force-time (b)-(e) and displacement-time (c)-(f) functions. (a)-(c) refer to the scaled El Centro earthquake multiplied by 0.5, while (d)-(f) to the unscaled earthquake (peak ground acceleration 0.349 g).

284 Fig.9 shows the response of the LTF system in Fig.6 under the El Centro earth-

285 quake. Fig.9(a)-(c) refers to the response under the El Centro earthquake uniformly
286 scaled by a 0.5 factor. Fig.9(d)-(e) reveal the response of the same system under
287 the unscaled earthquake. As anticipated, the system's response is very stable: the
288 upper and lower bounds are the experimental backbone. Both simulations mani-
289 fest the occurrence of pinching. However, the second is associated with a higher
290 displacement due to the exceeding of 30mm displacement. The stability of empir-
291 ical hysteresis models is essential and represents a crucial feature in evaluating its
292 performance. Differential hysteresis models are more prone to exhibit unstable re-
293 sponses than non-differential ones [43]. Additionally, several hysteresis models do
294 not manifest pinching under earthquake excitation. This result depends on the use
295 of the dissipated energy as a time-dependent parameter. The weaknesses related to
296 the use of the dissipated hysteretic energy are discussed in the following sections.
297 In conclusion, the proposed model presents a stable performance and can simulate
298 the structural response under pseudo-static and dynamic excitation.

299 4. Validation

300 This section deals with model validation. Firstly, the authors calibrate the model
301 on the experimental cyclic response of a given structural system. Then, the response
302 of the already calibrated model is compared to the experimental response of the same
303 structural system excited by a different input. Precisely, the authors used the exper-
304 imental cyclic response of plywood-coupled LVL wall panels detailed in [46]. Iqbal
305 et al. investigated the response of the same plywood-coupled LVL wall to pseudo-
306 static and pseudo-dynamic loading. The loading protocol adopted for pseudo-static
307 symmetric cyclic testing was a modification of ACI T1.1-01, ACI T1.1R-01 [47],
308 proposed for the testing on innovative jointed precast concrete frame systems.

309 Fig.10 presents the comparison between the experimental cyclic response of the
310 prestressed plywood-coupled LVL shear wall and the calibrated hysteresis model.
311 The shape of this system is also peculiar, characterized by more significant energy

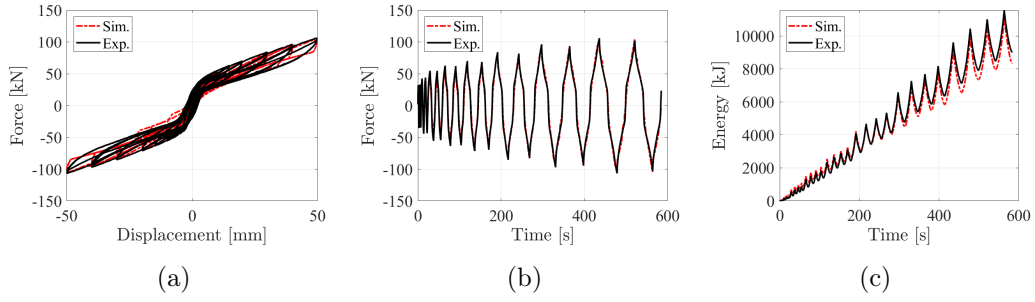


Figure 10: Comparison between the experimental cyclic response of a prestressed plywood-coupled LVL shear wall and the proposed model in term of force-displacement (a), force-time (b) and energy-time (c) functions. Exp. stands for experimental data, while Sim. for simulated data. Iqbal et al. provide full detail of the experimental setup in [46].

312 dissipation after the attainment of a displacement threshold. Accurately, a displace-
 313 ment approximately equal to 30mm is associated with a sudden stiffness decrement.
 314 The backbone resembles a sort of bi-linear function. However, the inclusion of the
 315 experimental data within the formulation does not entail an ad hoc definition of
 316 the first-loading path. The matching between the experimental and simulated re-
 317 sponse is very satisfactory, as proved by the force-time and energy-time functions
 318 in Fig.10(b)-(c). Tab.2 reports the optimized parameters and the associated error,
 319 comparable to the precedent cases.

Table 2: Model parameters, Root Mean Square error (rmse) and maximum error corresponding to the models in Figs.10,11. The error is the difference between the experimental and simulated force vectors.

Value	LVL pseudostatic	LVL pseudodynamic
$n_p^+ = n_p^-$	0.48	0.48
$n_s^+ = n_s^-$	0.81	0.81
$f_r^+ = f_r^-$ [kN]	10.3	10.3
Max error [kN]	33.6	35.63
RMSE [kN]	6.26	8.22

320 Fig.11 bestows the response of the real structural and the hybrid hysteresis model
 321 to pseudo-dynamic loading. The hysteresis model has been already calibrated, and
 322 the comparison between the two responses is a validation of the model: the scholar
 323 can theoretically use the model to extrapolate information using different inputs or,
 324 more generally, different structural configurations. Tab.2 proves that the error as-
 325 sociated with the pseudo-dynamic tests is not much higher than the one associated

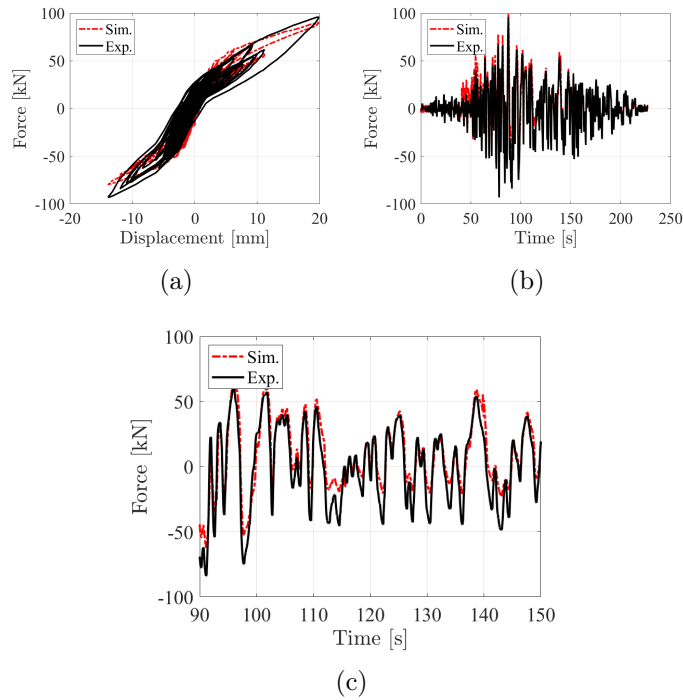


Figure 11: Comparison between the response of a prestressed plywood-coupled LVL shear wall and the proposed hybrid model under pseudo-dynamic tests in term of force-displacement (a), force-time (b) functions. Exp. stands for experimental data, while Sim. for simulated data; (c) is a detail of the force-time function in the central part of the plot in (b).

326 with the pseudo-static test. The model satisfactorily reproduces experimental data
 327 from cyclic tests, Fig.11. Consequently, experimental data could be considered ade-
 328 quately fitted for engineering purposes. In particular, the two responses are nearly
 329 coinciding in the central part of the graph, as evidenced in Fig.11(c).

330 5. Discussion: the role of the dissipated hysteretic energy

331 The proposed formulation has two pieces of novelties compared to existing ones.
 332 (i) The inclusion of the experimental backbone, leading to a hybrid, analytical-
 333 numerical hysteresis model. (ii) Adopting the sole maximum displacement as an
 334 evolutionary parameter, ignoring the dependence on dissipated hysteretic energy,
 335 often included in hysteresis models with degradation and pinching. Including the
 336 dissipated hysteretic energy can be valuable in certain circumstances, especially
 337 when the first-loading and re-loading paths have the same curvature sign [48]. How-
 338 ever, in some instances, it can lead to inconsistent results. The following paragraphs

339 attempt to explain the shortcomings possibly related to the use of the dissipated
 340 energy. In several formulations, like [3], the stiffness of the pinching path has the
 341 following exponential unfolding:

$$k_p \propto \exp(-\lambda\epsilon) \quad (6)$$

342 where λ is a coefficient and ϵ the dissipated hysteretic energy. The dissipated energy
 343 up to a given displacement value \hat{d} , corresponding to the k th integration step is:

$$\epsilon_k = \epsilon(\mathbf{d}_k) \quad (7)$$

344 where \mathbf{d}_k collects the simulated displacement. Therefore, if the experimenter uses
 345 different loading protocols $\mathbf{d}_{k,1} \neq \mathbf{d}_{k,2}$, the resulting dissipated energy $\epsilon_k(\mathbf{d}_{k,1}) \neq$
 346 $\epsilon_k(\mathbf{d}_{k,2})$ can be different given a certain displacement value \hat{d} . Suppose the scholar
 347 calibrates the hysteresis model on experimental data characterized by a given dis-
 348 placement protocol \mathbf{d}_1 . Then, the slope of the pinching path associated with a \hat{d}
 349 displacement is labeled $k_{p,1}$. However, if he estimates the model response using a
 350 displacement protocol different from the one used for calibration (\mathbf{d}_2), the slope of
 351 the pinching path associated with the same \hat{d} , $k_{p,2}$ can be different than $k_{p,1}$, specif-
 352 ically $k_{p,1} \neq k_{p,2}$. If \mathbf{d}_2 leads to a lower dissipated energy when $d_k = \hat{d}$, the estimate
 353 of the pinching slope is biased. Accurately, the adoption of a displacement protocol
 354 yielding a lower dissipation in \hat{d} leads to:

$$\hat{k}_{p,2} > \hat{k}_{p,1} \quad (8)$$

355 where $\hat{k}_{p,1}$ is the estimated stiffness based on the displacement protocol used for
 356 calibration (\mathbf{d}_1), while $\hat{k}_{p,1}$ is the estimated stiffness using a loading protocol (\mathbf{d}_2)
 357 associated with a lower dissipation in \hat{d} . The outgrowth of a biased stiffness estimate
 358 is an overestimation of the resisting force, surpassing the backbone curve. Fig.12

359 endeavours to illustrate this phenomenon. It shows two qualitative experimental
360 cyclic responses of the same structural system. The first descends from the repeti-
361 tion of multiple cycles (solid black line), the second derives from the repetition of
362 lower cycles (dashed red line). Reasonably, the slope of the pinching path can be
363 different in the two experimental situations. However, the resisting force associated
364 with a \hat{d} displacement must be lower than the backbone in both cases. However,
365 suppose the scholar adopts an exponential-like decaying of the stiffness depending
366 on the dissipated energy. In that case, the slope of the pinching path obtained
367 from a displacement d_2 can be overestimated. The k_p overestimation leads to the
368 exceeding of the backbone and inconsistent results.

369 This elementary example proves that adopting hysteretic energy as an evolutionary
370 parameter may lead to a paradox, the resisting force of the pinching paths surpasses
371 the backbone.

372 Most of the existing empirical hysteresis models use energy-based formulations.
373 However, this rudimentary analysis proves that the outcomes of these models may
374 be inconsistent if the scholar adopts a displacement protocol different from the
375 calibration one.

376

377 The pinching phenomenon mostly depends on damage accumulation, and the
378 dissipated hysteretic energy is an acknowledged indicator of progressive damage.
379 Some scholars, starting from the pioneering Bouc-Wen-Barber-Noori (BWBN)
380 model [2], do not define pinching using the sole maximum displacement. They
381 adopt an energy-based formulation, where the stiffness of the loading path depends
382 on the dissipated energy [49–51]. This formulation successfully works if the first-
383 loading and re-loading paths have the same curvature [52, 53]. If the structural
384 system manifests a curvature opposition between first-loading and re-loading, see
385 Fig.2, the results can be biased under different displacement protocols.

386

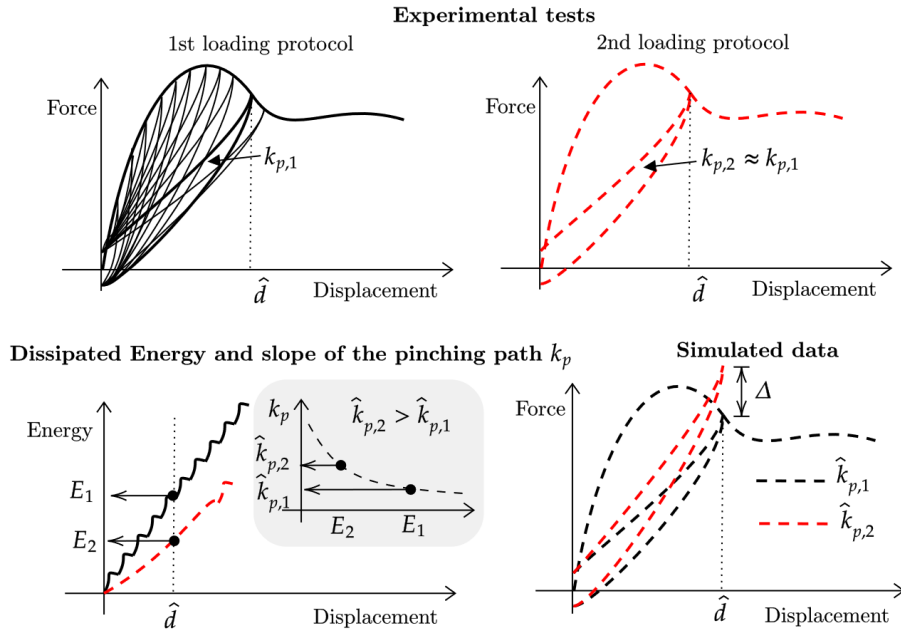


Figure 12: Illustration of the shortcomings possibly associated with energy-based formulations of degradation phenomena in empirical hysteresis models.

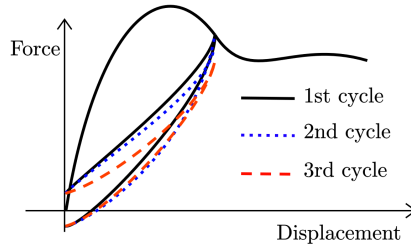


Figure 13: Effect of the dissipated hysteretic energy on multiple cycles.

387 Nevertheless, numerous experimental tests on different structural systems (re-
 388 inforced concrete [54–57], timber [45, 58–61], masonry [62–65], e.g.) demonstrated
 389 that the slope of the pinching path chiefly depends on the maximum displacement
 390 rather than on the dissipated energy. Fig.13 attempts to explain the effect of dis-
 391 sipated hysteretic energy on multiple cycles. Specifically, the EN 594:2011 protocol
 392 includes the repetition of three cycles with the same amplitude. In most cases [66–
 393 74], what illustrated in Fig.13 appears. The repetition of the same cycle never yields
 394 force values higher than the backbone. The pinching and unloading paths slope can
 395 be different, possibly generating a lower force value (identified as a pinching fraction,
 396 q , [3]). However, the 2nd and 3rd cycles are very similar in most situations, like

397 the ones displayed in Fig.6,7,8. Consequently, if the hysteresis model should have a
 398 limited number of parameters, the dissipated energy could be ignored. It yields mi-
 399 nor effects compared to those associated with the maximum attained displacement.
 400 The current paper proves that a hysteresis model based on the sole definition of the
 401 maximum displacement can yield a satisfactory agreement with the experimental
 402 data for engineering purposes.

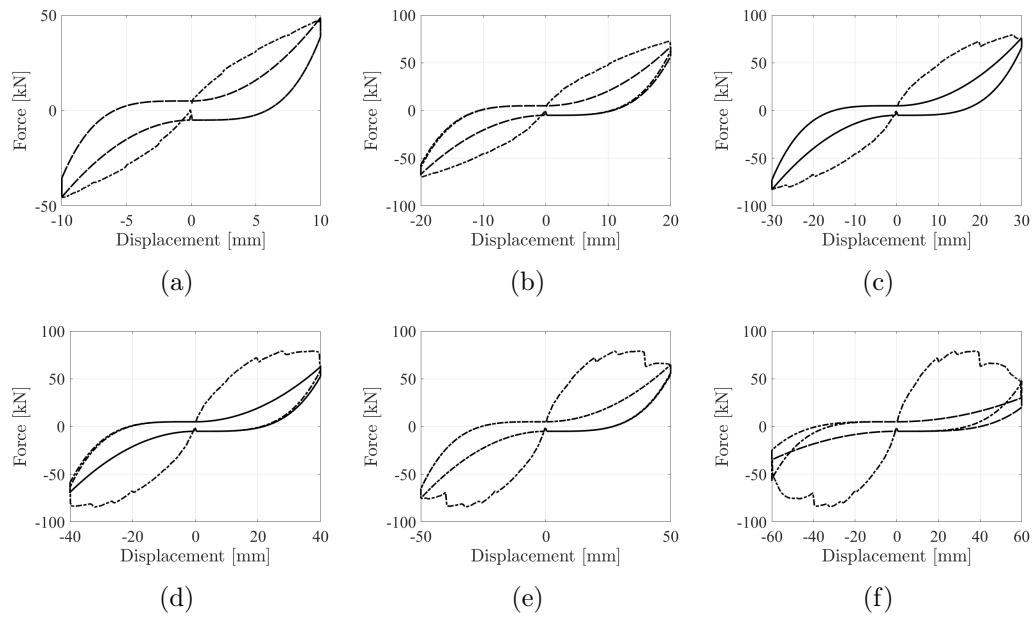


Figure 14: Cyclic response of of the LTF model in Fig.6 using sinusoidal imposed displacement with growing amplitude from (a) to (f).

403 Fig.14 shows the response of the LTF model under sinusoidal excitation, grow-
 404 ing from 10 to 60mm. Fig.14 proves that the model return consistent results, upper
 405 bounded by the backbone, under displacement protocols different from the calibra-
 406 tion ones.

407 6. Conclusions

408 The current paper presents an alternative way to empirical hysteresis modelling
 409 in structural engineering. The need for empirical hysteresis models originates from
 410 the necessity to estimate the inelastic response of complex structural arrangements
 411 without adopting a whole Finite Element approach. Finite Element analyses would

412 entail time-consuming simulations, possibly impractical in working applications and
413 some research activities. The authors propose a non-differential hysteresis model
414 based on the partition of the hysteresis loop into six parts, distinguished by the
415 signs of velocity and displacement and the past displacement history. The formula-
416 tion has two significant pieces of novelties. (i) The first-loading paths originate from
417 the experimental backbone by solving a step-by-step optimization problem. (ii) The
418 evolution of degradation phenomena is driven by time-variant coefficients, where
419 the sole maximum attained displacement and not the dissipated hysteretic energy
420 determine the strength and stiffness evolution. This choice derives from possible
421 weaknesses in using the dissipated hysteretic energy as a degradation parameter un-
422 der input displacements different from the experimental ones. The proposed model
423 is defined as a hybrid, being the product of an analytical formulation and the out-
424 come of an optimization problem. The advantages in using this model stand in the
425 limited number of unknown parameters, six, and the significant stability of time-
426 integration under non-stationary inputs. The quality of a hysteresis model derives
427 from balancing accuracy and the number of governing parameters. The best model
428 should achieve a good correspondence with the lowest number of parameters. The
429 authors proved the model versatility on three experimental cyclic responses. Then,
430 they validated the model on the experimental response of a structural system under
431 different displacement inputs. The model faithfully reproduces the experimental
432 data and can represent a valid alternative to traditional empirical hysteresis models
433 based on an entire analytical approach. The authors developed the model in Matlab.
434 In the appendix, the reader can find the implemented code for displacement-driven
435 simulations.

436 **References**

- 437 [1] A. Aloisio, R. Alaggio, J. Köhler, and M. Fragiaco, “Extension of generalized bouc-wen
438 hysteresis modeling of wood joints and structural systems,” *Journal of Engineering Mechanics*,
439 vol. 146, no. 3, p. 04020001, 2020.

- 440 [2] T. T. Baber and M. N. Noori, "Random vibration of degrading, pinching systems," *Journal*
441 *of Engineering Mechanics*, vol. 111, no. 8, pp. 1010–1026, 1985.
- 442 [3] G. C. Foliente, "Hysteresis modeling of wood joints and structural systems," *Journal of Struc-*
443 *tural Engineering*, vol. 121, no. 6, pp. 1013–1022, 1995.
- 444 [4] J. Song and A. Der Kiureghian, "Generalized bouc–wen model for highly asymmetric hystere-
445 sis," *Journal of engineering mechanics*, vol. 132, no. 6, pp. 610–618, 2006.
- 446 [5] S. Sirotti, M. Pellicciari, F. Di Trapani, B. Briseghella, G. Carlo Marano, C. Nuti, and A. M.
447 Tarantino, "Development and validation of new bouc–wen data-driven hysteresis model for
448 masonry infilled rc frames," *Journal of Engineering Mechanics*, vol. 147, no. 11, p. 04021092,
449 2021.
- 450 [6] R. Bouc, "Solution periodique de lequation de la ferroresonance avec hysteresis," *COMPTE*
451 *RENDUS HEBDOMADAIRES DES SEANCES DE L ACADEMIE DES SCIENCES SERIE*
452 *A*, vol. 263, no. 15, p. 497, 1966.
- 453 [7] M. Ismail, F. Ikhoulane, and J. Rodellar, "The hysteresis bouc-wen model, a survey," *Archives*
454 *of Computational Methods in Engineering*, vol. 16, no. 2, pp. 161–188, 2009.
- 455 [8] W. Pu, C. Liu, and F. Dai, "Optimum hysteretic damper design for multi-story timber
456 structures represented by an improved pinching model," *Bulletin of Earthquake Engineering*,
457 vol. 16, no. 12, pp. 6221–6241, 2018.
- 458 [9] A. Di Cesare, F. C. Ponzio, S. Pampanin, T. Smith, D. Nigro, and N. Lamarucciola, "Dis-
459 placement based design of post-tensioned timber framed buildings with dissipative rocking
460 mechanism," *Soil Dynamics and Earthquake Engineering*, vol. 116, pp. 317–330, 2019.
- 461 [10] A. Aloisio, M. Pellicciari, A. V. Bergami, R. Alaggio, B. Briseghella, and M. Fragiaco,
462 "Effect of pinching on structural resilience: performance of reinforced concrete and timber
463 structures under repeated cycles," *Structure and Infrastructure Engineering*, pp. 1–17, 2022.
- 464 [11] A. Aloisio, M. Pellicciari, R. Alaggio, C. Nuti, M. Fragiaco, and B. Briseghella, "Structural
465 robustness of an rc pier under repeated earthquakes," in *Proceedings of the Institution of Civil*
466 *Engineers-Bridge Engineering*, pp. 1–20, Thomas Telford Ltd, 2021.
- 467 [12] W. Ramberg and W. R. Osgood, "Description of stress-strain curves by three parameters,"
468 1943.
- 469 [13] M. Menegotto, "Method of analysis for cyclically loaded rc plane frames including changes in
470 geometry and non-elastic behavior of elements under combined normal force and bending,"
471 in *Proc. of IABSE symposium on resistance and ultimate deformability of structures acted on*
472 *by well defined repeated loads*, pp. 15–22, 1973.
- 473 [14] N. Vaiana, F. Marmo, S. Sessa, and L. Rosati, "Modeling of the hysteretic behavior of wire

- 474 rope isolators using a novel rate-independent model,” in *Nonlinear Dynamics of Structures,*
475 *Systems and Devices*, pp. 309–317, Springer, 2020.
- 476 [15] A. Pacitti, M. Peigney, F. Bourquin, and W. Lacarbonara, “Experimental data based cable
477 tension identification via nonlinear static inverse problem,” *Procedia engineering*, vol. 199,
478 pp. 453–458, 2017.
- 479 [16] A. Tatar and D. M. Dowden, “Analytical and numerical investigation of a low-damage uplift
480 friction damper for self-centering cross-laminated timber rocking walls,” *Engineering Struc-*
481 *tures*, vol. 254, p. 113836, 2022.
- 482 [17] A. Aloisio, M. Pelliciani, S. Sirotti, F. Boggian, and R. Tomasi, “Optimization of the structural
483 coupling between rc frames, clt shear walls and asymmetric friction connections,” *Bulletin of*
484 *Earthquake Engineering*, pp. 1–26, 2022.
- 485 [18] A. Aloisio, F. Boggian, and R. Tomasi, “Design of a novel seismic retrofitting system for rc
486 structures based on asymmetric friction connections and clt panels,” *Engineering Structures*,
487 vol. 254, p. 113807, 2022.
- 488 [19] A. Aloisio, F. Boggian, R. Tomasi, and M. Fragiacomò, “Reliability-based assessment of ltf and
489 clt shear walls under in-plane seismic loading using a modified bouc-wen hysteresis model,”
490 *ASCE-ASME Journal of Risk and Uncertainty in Engineering Systems, Part A: Civil Engi-*
491 *neering*, vol. 7, no. 4, p. 04021065, 2021.
- 492 [20] B. Kivell, P. Moss, and A. Carr, “Hysteretic modelling of moment-resisting nailed timber
493 joints,” *Earthquake Engineering*, vol. 14, no. 4, 1981.
- 494 [21] D. Dowrick, “Hysteresis loops for timber structures,” *Bulletin of the New Zealand Society for*
495 *Earthquake Engineering*, vol. 19, no. 2, pp. 143–152, 1986.
- 496 [22] M. He, F. Lam, and R. O. Foschi, “Modeling three-dimensional timber light-frame buildings,”
497 *Journal of Structural Engineering*, vol. 127, no. 8, pp. 901–913, 2001.
- 498 [23] J.-Q. Yang, S. T. Smith, Z. Wang, P. Feng, and N. Sirach, “Modelling of hysteresis behaviour
499 of moment-resisting timber joints strengthened with frp composites,” *International Journal*
500 *of Mechanical Sciences*, p. 105593, 2020.
- 501 [24] H. T. Nguyen and S. E. Kim, “Finite element modeling of push-out tests for large stud shear
502 connectors,” *Journal of Constructional Steel Research*, vol. 65, no. 10-11, pp. 1909–1920, 2009.
- 503 [25] T. Gečys, A. Daniūnas, T. K. Bader, L. Wagner, and J. Eberhardsteiner, “3d finite element
504 analysis and experimental investigations of a new type of timber beam-to-beam connection,”
505 *Engineering structures*, vol. 86, pp. 134–145, 2015.
- 506 [26] A. Hassanieh, H. Valipour, M. Bradford, and C. Sandhaas, “Modelling of steel-timber com-
507 posite connections: Validation of finite element model and parametric study,” *Engineering*

- 508 *Structures*, vol. 138, pp. 35–49, 2017.
- 509 [27] C. Bedon and M. Fragiacomò, “Numerical analysis of timber-to-timber joints and composite
510 beams with inclined self-tapping screws,” *Composite Structures*, vol. 207, pp. 13–28, 2019.
- 511 [28] C. Bedon, G. Rinaldin, M. Fragiacomò, and S. Noé, “q-factor estimation for 3d log-house
512 timber buildings via finite element analyses,” *Soil Dynamics and Earthquake Engineering*,
513 vol. 116, pp. 215–229, 2019.
- 514 [29] Y. De Santis and M. Fragiacomò, “Timber-to-timber and steel-to-timber screw connections:
515 Derivation of the slip modulus via beam on elastic foundation model,” *Engineering Structures*,
516 vol. 244, p. 112798, 2021.
- 517 [30] J. Humbert, C. Boudaud, J. Baroth, S. Hameury, and L. Daudeville, “Joints and wood shear
518 walls modelling i: Constitutive law, experimental tests and fe model under quasi-static load-
519 ing,” *Engineering Structures*, vol. 65, pp. 52–61, 2014.
- 520 [31] K. Vogrinec, M. Premrov, and E. K. Šilih, “Simplified modelling of timber-framed walls under
521 lateral loads,” *Engineering structures*, vol. 111, pp. 275–284, 2016.
- 522 [32] J. Jayamon, F. Charney, F. Flores, and P. Line, “Influence of wall load-displacement shape
523 on seismic performance of wood-frame shear wall structures,” in *World Conference on Timber*
524 *Engineering*, 2016.
- 525 [33] Ö. Anil, A. Togay, Ü. K. İşleyen, N. Döngel, and C. Söğütü, “Effect of timber type and nail
526 spacing on the hysteretic behavior of timber-framed shear walls with openings,” *International*
527 *Journal of Civil Engineering*, vol. 16, no. 6, pp. 629–646, 2018.
- 528 [34] A. Polensek and H. I. Laursen, *Seismic Behavior of Bending Components and Intercomponent*
529 *Connections of Light Frame Wood Buildings*. Oregon State University, 1984.
- 530 [35] G. Rinaldin, C. Amadio, and M. Fragiacomò, “A component approach for the hysteretic
531 behaviour of connections in cross-laminated wooden structures,” *Earthquake engineering &*
532 *structural dynamics*, vol. 42, no. 13, pp. 2023–2042, 2013.
- 533 [36] G. Di Gangi, C. Demartino, G. Quaranta, and G. Monti, “Dissipation in sheathing-to-framing
534 connections of light-frame timber shear walls under seismic loads,” *Engineering Structures*,
535 vol. 208, p. 110246, 2020.
- 536 [37] B. Folz and A. Filiatrault, “Seismic analysis of woodframe structures. i: Model formulation,”
537 *Journal of Structural Engineering*, vol. 130, no. 9, pp. 1353–1360, 2004.
- 538 [38] W. Pang, D. Rosowsky, S. Pei, and J. Van de Lindt, “Evolutionary parameter hysteretic model
539 for wood shear walls,” *Journal of structural engineering*, vol. 133, no. 8, pp. 1118–1129, 2007.
- 540 [39] J. P. Judd and F. S. Fonseca, “Analytical model for sheathing-to-framing connections in wood
541 shear walls and diaphragms,” *Journal of structural engineering*, vol. 131, no. 2, pp. 345–352,

- 542 2005.
- 543 [40] A. Blasetti, R. Hoffman, and D. Dinehart, “Simplified hysteretic finite-element model for
544 wood and viscoelastic polymer connections for the dynamic analysis of shear walls,” *Journal*
545 *of structural engineering*, vol. 134, no. 1, pp. 77–86, 2008.
- 546 [41] J. D. Dolan, *The dynamic response of timber shear walls*. PhD thesis, University of British
547 Columbia, 1989.
- 548 [42] J. Xu and J. D. Dolan, “Development of nailed wood joint element in abaqus,” *Journal of*
549 *structural engineering*, vol. 135, no. 8, pp. 968–976, 2009.
- 550 [43] A. Aloisio, P. Sejkot, A. Iqbal, and M. Fragiaco, “An empirical transcendental hystere-
551 sis model for structural systems with pinching and degradation,” *Earthquake Engineering &*
552 *Structural Dynamics*, 2021.
- 553 [44] P. Grossi, T. Sartori, and R. Tomasi, “Tests on timber frame walls under in-plane forces: part
554 2,” *Proceedings of the Institution of Civil Engineers-Structures and Buildings*, vol. 168, no. 11,
555 pp. 840–852, 2015.
- 556 [45] A. Aloisio, F. Boggian, T. Roberto, and M. Fragiaco, “The role of the hold-down in the
557 capacity model of clt andltf shear walls based on the experimental lateral response,” *Con-*
558 *struction and Building Materials*, vol. In press, 2021.
- 559 [46] A. Iqbal, M. Fragiaco, S. Pampanin, and A. Buchanan, “Seismic resilience of plywood-
560 coupled lvl wall panels,” *Engineering Structures*, vol. 167, pp. 750–759, 2018.
- 561 [47] A. I. T. G. 1, “Acceptance criteria for moment frames based on structural testing (t1. 1-01)
562 and commentary (t1. 1r-01): An aci standard,” American Concrete Institute, 2001.
- 563 [48] M. Pellicciari, B. Briseghella, F. Tondolo, L. Veneziano, C. Nuti, R. Greco, D. Lavorato,
564 and A. M. Tarantino, “A degrading bouc–wen model for the hysteresis of reinforced concrete
565 structural elements,” *Structure and Infrastructure Engineering*, vol. 16, no. 7, pp. 917–930,
566 2020.
- 567 [49] G. A. Ortiz, D. A. Alvarez, and D. Bedoya-Ruíz, “Identification of bouc–wen type models
568 using multi-objective optimization algorithms,” *Computers & Structures*, vol. 114, pp. 121–
569 132, 2013.
- 570 [50] G. Peng, W. Li, H. Du, H. Deng, and G. Alici, “Modelling and identifying the parameters of a
571 magneto-rheological damper with a force-lag phenomenon,” *Applied Mathematical Modelling*,
572 vol. 38, no. 15-16, pp. 3763–3773, 2014.
- 573 [51] G. Marano, M. Pellicciari, T. Cuoghi, B. Briseghella, D. Lavorato, and A. Tarantino, “De-
574 grading bouc–wen model parameters identification under cyclic load,” *International Journal*
575 *of Geotechnical Earthquake Engineering (IJGEE)*, vol. 8, no. 2, pp. 60–81, 2017.

- 576 [52] A. Manzoori and H. Toopchi-Nezhad, "Application of an extended bouc-wen model in seismic
577 response prediction of unbonded fiber-reinforced isolators," *Journal of Earthquake Engineer-*
578 *ing*, vol. 21, no. 1, pp. 87–104, 2017.
- 579 [53] V. Niola, G. Palli, S. Strano, and M. Terzo, "Nonlinear estimation of the bouc-wen model with
580 parameter boundaries: Application to seismic isolators," *Computers & Structures*, vol. 222,
581 pp. 1–9, 2019.
- 582 [54] F. Colangelo, "Pseudo-dynamic seismic response of reinforced concrete frames infilled with
583 non-structural brick masonry," *Earthquake engineering & structural dynamics*, vol. 34, no. 10,
584 pp. 1219–1241, 2005.
- 585 [55] A. B. Mehrabi, P. Benson Shing, M. P. Schuller, and J. L. Noland, "Experimental evaluation
586 of masonry-infilled rc frames," *Journal of Structural engineering*, vol. 122, no. 3, pp. 228–237,
587 1996.
- 588 [56] L. Cavaleri and F. Di Trapani, "Cyclic response of masonry infilled rc frames: Experimental
589 results and simplified modeling," *Soil Dynamics and Earthquake Engineering*, vol. 65, pp. 224–
590 242, 2014.
- 591 [57] A. V. Bergami and C. Nuti, "Experimental tests and global modeling of masonry infilled
592 frames," *Earthquakes and Structures*, vol. 9, no. 2, pp. 281–303, 2015.
- 593 [58] I. Gavric, M. Fragiaco, and A. Ceccotti, "Cyclic behavior of clt wall systems: Experimental
594 tests and analytical prediction models," *Journal of Structural Engineering*, vol. 141, no. 11,
595 p. 04015034, 2015.
- 596 [59] J. Schneider, Y. Shen, S. Stiemer, and S. Tesfamariam, "Assessment and comparison of exper-
597 imental and numerical model studies of cross-laminated timber mechanical connections under
598 cyclic loading," *Construction and Building Materials*, vol. 77, pp. 197–212, 2015.
- 599 [60] R. Tomasi and T. Sartori, "Mechanical behaviour of connections between wood framed shear
600 walls and foundations under monotonic and cyclic load," *Construction and Building Materials*,
601 vol. 44, pp. 682–690, 2013.
- 602 [61] A. Aloisio, R. Alaggio, and M. Fragiaco, "Equivalent viscous damping of cross-laminated
603 timber structural archetypes," *Journal of Structural Engineering*, vol. 147, no. 4, p. 04021012,
604 2021.
- 605 [62] M. Angiolilli and A. Gregori, "Triplet test on rubble stone masonry: Numerical assessment of
606 the shear mechanical parameters," *Buildings*, vol. 10, no. 3, p. 49, 2020.
- 607 [63] G. Vasconcelos and P. B. Lourenço, "In-plane experimental behavior of stone masonry walls
608 under cyclic loading," *Journal of structural engineering*, vol. 135, no. 10, pp. 1269–1277, 2009.
- 609 [64] S. M. Nolph and M. A. ElGawady, "Static cyclic response of partially grouted masonry shear

- walls,” *Journal of structural engineering*, vol. 138, no. 7, pp. 864–879, 2012.
- [65] D. Malomo, M. J. DeJong, and A. Penna, “Distinct element modelling of the in-plane cyclic response of urm walls subjected to shear-compression,” *Earthquake Engineering & Structural Dynamics*, vol. 48, no. 12, pp. 1322–1344, 2019.
- [66] Z. Li, X. Zheng, M. He, Y. Sun, and G. He, “Experimental and analytical investigations into the time-dependent performance in post-tensioned timber beam-column joints under sustained loads and varied environment,” *Construction and Building Materials*, vol. 251, p. 118943, 2020.
- [67] B. Shi, W. Zhu, H. Yang, W. Liu, H. Tao, and Z. Ling, “Experimental and theoretical investigation of prefabricated timber-concrete composite beams with and without prestress,” *Engineering Structures*, vol. 204, p. 109901, 2020.
- [68] H. Mpidi Bitá and T. Tannert, “Experimental study of disproportionate collapse prevention mechanisms for mass-timber floor systems,” *Journal of Structural Engineering*, vol. 146, no. 2, p. 04019199, 2020.
- [69] S. Miller, J. E. Woods, J. Erochko, D. T. Lau, and C. F. Gilbert, “Experimental and analytical fragility assessment of a combined heavy timber–steel-braced frame through hybrid simulation,” *Earthquake Engineering & Structural Dynamics*, 2020.
- [70] F. Alinoori, P. Sharafi, F. Moshiri, and B. Samali, “Experimental investigation on load bearing capacity of full scaled light timber framed wall for mid-rise buildings,” *Construction and Building Materials*, vol. 231, p. 117069, 2020.
- [71] A. Di Cesare, F. C. Ponzó, N. Lamarucciola, and D. Nigro, “Experimental seismic response of a resilient 3-storey post-tensioned timber framed building with dissipative braces,” *Bulletin of Earthquake Engineering*, pp. 1–24, 2020.
- [72] H. Bagheri, A. Hashemi, S. Yousef-Beik, P. Zarnani, and P. Quenneville, “New self-centering tension-only brace using resilient slip-friction joint: Experimental tests and numerical analysis,” *Journal of Structural Engineering*, vol. 146, no. 10, p. 04020219, 2020.
- [73] S. Guo, M. He, Z. Li, F. Liang, F. Chen, Y. Sun, B. Briseghella, and G. He, “Lateral performance of midply wood shear walls with anchor tie-down system: Experimental investigation and numerical simulation,” *Construction and Building Materials*, vol. 235, p. 117518, 2020.
- [74] I. Lukacs, A. Björnfort, and R. Tomasi, “Strength and stiffness of cross-laminated timber (clt) shear walls: State-of-the-art of analytical approaches,” *Engineering Structures*, vol. 178, pp. 136–147, 2019. cited By 14.

641 7. Acknowledgments

642 The authors acknowledge the significant contribution of Prof. Roberto Tomasi,
643 who provided us with the experimental data of CLT and LTF shear walls.

644 This work has been supported by the Ministry of Culture of the Czech Republic,
645 research grant NAKI II DG18P02OVV012 - Sustainable Management of Historical
646 Buildings.

647 8. Appendix

648 Below the reader can find the Matlab code of the hysteresis model presented in
649 this paper.

```
650 1
651 2 %% INPUT DATA
652 3 %Db1=Positive backbone displacements
653 4 %Db2=Negative backbone displacements
654 5 %Fb1=Positive backbone forces
655 6 %Fb2=Negative backbone forces
656 7 %x= Imposed displacement
657 8 fr=2;
658 9 ns=6;
659 10 np=3;
660 11 %% OUTPUT DATA
661 12 %Fs Simulated Force
662 13 %% CODE
663 14 for k=2:size(x,1)
664 15 if abs(x(k))>abs(x(k-1)) && (x(k))>=max(x(1:k-1)) && x(k)>0 %PHASE 1
665 16 [C,I] = min(((x(k)-Db1)).^2);
666 17 Fs(k)=Fb1(I);
667 18 elseif abs(x(k))>abs(x(k-1)) && (x(k))>min(x(1:k-1))&& x(k)<0 %PHASE 2
668 19 [C,I] = min(((min(x(1:k-1))-Db2)).^2);
669 20 Fs(k)=(((Fb2(I)+fr)/(abs(min(x(1:k-1))))^np))*(abs(x(k)))^np)-fr;
670 21 elseif abs(x(k))<abs(x(k-1))&& x(k)>0 %PHASE 3
671 22 TF = islocalmax(Fs(1:k));
672 23 F=Fs(1:k);
673 24 Fm=vertcat(max(Fs(1:k)),F(TF));
674 25 TF = islocalmax(x(1:k));
675 26 X=x(1:k);
676 27 Xm=vertcat(max(x(1:k)),X(TF));
677 28 Fs(k)=((Fm(size(Fm,1))-fr)/((abs(Xm(size(Xm,1))))^ns))*(abs(x(k)))^ns-fr;
678 29 elseif abs(x(k))>abs(x(k-1)) && (x(k))<=min(x(1:k-1)) && x(k)<0 %PHASE 4
679 30 [C,I] = min(((x(k)-Db2)).^2);
680 31 Fs(k)=Fb2(I);
681 32 elseif abs(x(k))>abs(x(k-1)) && (x(k))<max(x(1:k-1))&& x(k)>0 %PHASE 5
682 33 [C,I] = min(((max(x(1:k-1))-Db1)).^2);
683 34 Fs(k)=(((Fb1(I)-fr)/(abs(max(x(1:k-1))))^np))*(abs(x(k)))^np)+fr;
```

```

685 35 elseif abs(x(k))<abs(x(k-1))&& x(k)<0 %PHASE 6
686 36 TF = islocalmin(Fs(1:k));
687 37 F=Fs(1:k);
688 38 Fm=vertcat(min(F(1:k)),F(TF));
689 39 TF = islocalmin(x(1:k));
690 40 X=x(1:k);
691 41 Xm=vertcat(min(x(1:k)),X(TF));
692 42 Fs(k)=((Fm(size(Fm,1))+fr)/((abs(Xm(size(Xm,1))))^ns))*(abs(x(k)))^ns+fr);
693 43 else
694 44 Fs(k)=Fs(k-1);
695 45 end
696 46 end
697

```

698 Below the reader can find the Python code of the hysteresis model presented in
699 this paper.

```

700
701 1 #%% Importing libraries , Python version: 3.7.10
702 2 # Packages versions:
703 3 # numpy 1.19.5
704 4 # matplotlib 3.4.2
705 5 # scipy 1.7.0
706 6 import numpy as np
707 7 import matplotlib.pyplot as plt
708 8 from scipy.signal import find_peaks
709 9
710 10 #%% INPUT DATA
711 11 # Db1=Positive backbone displacements
712 12 # Db2=Negative backbone displacements
713 13 # Fb1=Positive backbone forces
714 14 # Fb2=Negative backbone forces
715 15 # x= Imposed displacement
716 16 fr=2
717 17 ns=6
718 18 n_p=3
719 19
720 20 #%% OUTPUT DATA
721 21 # Fs Simulated Force
722 22
723 23 #%% CODE
724 24 from scipy.signal import find_peaks
725 25
726 26 for k in range(1,np.shape(x)[0]):
727 27 #PHASE 1
728 28 if abs(x[k])>abs(x[k-1]) and (x[k])>=max(x[:k]) and x[k]>0 :
729 29 C = min(np.power([x[k]-Db1],2))
730 30 I = np.argmax(np.power([x[k]-Db1],2))
731 31 Fs[k]=Fb1[I]
732 32 #PHASE 2
733 33 elif abs(x[k])>abs(x[k-1]) and (x[k])>min(x[:k]) and x[k]<0 :
734 34 C = min(np.power(min(x[:k])-Db2,2))
735 35 I = np.argmax(np.power(min(x[:k])-Db2,2))
736 36 Fs[k]=(((Fb2[I]+fr)/(np.power(abs(min(x[:k])),n_p))))
737 37 *np.power(abs(x[k]),n_p))-fr
738 38 #PHASE 3

```

```

739 39     elif abs(x[k])<abs(x[k-1]) and x[k]>0 :
740 40         TF, _ = find_peaks(Fs[:k+1], height=0)
741 41         F = np.copy(Fs[:k+1])
742 42         Fm = np.hstack((max(Fs[:k+1]),F[TF]))
743 43         TF, _ = find_peaks(x[:k+1], height=0)
744 44         X=np.copy(x[:k+1])
745 45         Xm = np.hstack((max(x[:k+1]),X[TF]))
746 46         Fs[k]=((Fm[np.shape(Fm)[0]-1]-fr)/(np.power(abs(Xm[np.shape(Xm)[0]-1]),ns)))
747 47         *np.power(abs(x[k]),ns)-fr
748 48     #PHASE 4
749 49     elif abs(x[k])>abs(x[k-1]) and (x[k])≤min(x[:k]) and x[k]<0 :
750 50         C = min(np.power(x[k]-Db2,2))
751 51         I = np.argmin(np.power(x[k]-Db2,2))
752 52         Fs[k]=Fb2[I]
753 53     #PHASE 5
754 54     elif abs(x[k])>abs(x[k-1]) and (x[k])<max(x[:k]) and x[k]>0 :
755 55         C = min(np.power([max(x[:k])-Db1],2))
756 56         I = np.argmin(np.power([max(x[:k])-Db1],2))
757 57         Fs[k]=(((Fb1[I]-fr)/np.power(abs(max(x[:k])),n_p))
758 58             *np.power(abs(x[k]),n_p))+fr
759 59     #PHASE 6
760 60     elif abs(x[k])<abs(x[k-1]) and x[k]<0 :
761 61         TF, _ = find_peaks(-Fs[:k+1], height=0)
762 62         F = np.copy(Fs[:k+1])
763 63         Fm = np.hstack((min(F[:k+1]),F[TF]))
764 64         TF, _ = find_peaks(-x[:k+1], height=0)
765 65         X=np.copy(x[:k+1])
766 66         Xm=np.hstack((min(x[:k+1]),X[TF]))
767 67         Fs[k]=((Fm[np.shape(Fm)[0]-1]+fr)/(np.power(abs(Xm[np.shape(Xm)[0]-1]),ns)))
768 68         *np.power(abs(x[k]),ns)+fr
769 69     else :
770 70         Fs[k]=Fs[k-1]
771 71
772 72 # %% Plotting section
773 73
774 74 figure1 = plt.figure(1)
775 75 w=5 # windows width for moving_mean
776 76 moving_mean = np.convolve(Fs, np.ones(w), 'same') / w
777 77 plt.plot(x,moving_mean,lw=2,ls="dashdot",color="red")
778 78 plt.plot(x,Fo,lw=2,color="black")
779 79 plt.ylabel('Force [kN]',fontdict=font_labels)
780 80 plt.xlabel('Displacement [mm]',fontdict=font_labels)
781 81 plt.title('',fontdict=font_titles)
782 82 plt.grid(visible=True, which='major', axis='both')
783 83 plt.legend(['Sim.', 'Exp.'],loc="upper left",fontsize=16)
784 84 plt.tight_layout()
785 85 plt.savefig('CLT_1.png')
786 86
787 87 figure2 = plt.figure(2)
788 88 t = np.arange(0,np.shape(Fo)[0])*0.2
789 89 plt.plot(t,moving_mean,lw=2,ls="dashdot",color="red")
790 90 plt.plot(t,Fo,lw=2,color="black")
791 91 plt.ylabel('Force [kN]',fontdict=font_labels)
792 92 plt.xlabel('Time [s]',fontdict=font_labels)
793 93 plt.title('',fontdict=font_titles)
794 94 plt.grid(visible=True, which='major', axis='both')
795 95 plt.legend(['Sim.', 'Exp.'],loc="upper right",fontsize=16)
796 96 plt.tight_layout()

```

```
797 | 97 plt.savefig('CLT_2.png')
798 | 98
799 | 99 E = np.cumsum(Fo*np.hstack((np.diff(D),0)))
800 | 100 Es = np.cumsum(Fs*np.hstack((np.diff(D),0)))
801 | 101 figure3 = plt.figure(3)
802 | 102 plt.plot(t,Es,lw=2,ls="dashdot",color="red")
803 | 103 plt.plot(t,E,lw=2,color="black")
804 | 104 plt.ylabel('Energy [kJ]',fontdict=font_labels)
805 | 105 plt.xlabel('Time [s]',fontdict=font_labels)
806 | 106 plt.title('',fontdict=font_titles)
807 | 107 plt.grid(visible=True, which='major', axis='both')
808 | 108 plt.legend(['Sim.', 'Exp.'], loc="upper left", fontsize=16)
809 | 109 plt.tight_layout()
810 | 110 plt.savefig('CLT_3.png')
```